Journal of Biomedical Optics

BiomedicalOptics.SPIEDigitalLibrary.org

Intraoperative imaging during Mohs surgery with reflectance confocal microscopy: initial clinical experience

Eileen S. Flores
Miguel Cordova
Kivanc Kose
William Phillips
Anthony Rossi
Kishwer Nehal
Milind Rajadhyaksha

SPIE.

Journal of Biomedical Optics 20(6), 061103 (June 2015)

Intraoperative imaging during Mohs surgery with reflectance confocal microscopy: initial clinical experience

Eileen S. Flores,* Miguel Cordova, Kivanc Kose, William Phillips, Anthony Rossi, Kishwer Nehal,† and Milind Rajadhyaksha†
Memorial Sloan Kettering Cancer Center, Dermatology Service, New York, New York 10022, United States

Abstract. Mohs surgery for the removal of nonmelanoma skin cancers (NMSCs) is performed in stages, while being guided by the examination for residual tumor with frozen pathology. However, preparation of frozen pathology at each stage is time consuming and labor intensive. Real-time intraoperative reflectance confocal microscopy (RCM), combined with video mosaicking, may enable rapid detection of residual tumor directly in the surgical wounds on patients. We report our initial experience on 25 patients, using aluminum chloride for nuclear contrast. Imaging was performed in quadrants in the wound to simulate the Mohs surgeon's examination of pathology. Images and videos of the epidermal and dermal margins were found to be of clinically acceptable quality. Bright nuclear morphology was identified at the epidermal margin and detectable in residual NMSC tumors. The presence of residual tumor and normal skin features could be detected in the peripheral and deep dermal margins. Intraoperative RCM imaging may enable detection of residual tumor directly on patients during Mohs surgery, and may serve as an adjunct for frozen pathology. Ultimately, for routine clinical utility, a stronger tumor-to-dermis contrast may be necessary, and also a smaller microscope with an automated approach for imaging in the entire wound in a rapid and controlled manner. [DOI: 10.1117/1.JBO.20.6.061103]

Keywords: reflectance confocal microscopy; nonmelanoma skin cancer; Mohs surgery; intraoperative imaging; basal cell carcinoma; squamous cell carcinoma; video-mosaicking.

Paper 140641SSPR received Oct. 1, 2014; accepted for publication Dec. 4, 2014; published online Feb. 23, 2015.

1 Introduction

Nonmelanoma skin cancer (NMSC) is the most common malignancy and poses a public health burden in the United States (US) and worldwide.[1,2] Approximately 3.5 million new cases of NMSCs are diagnosed every year in the US. Of these, about 80% are basal cell carcinomas (BCCs) and the remaining are squamous cell carcinomas (SCCs). Mohs micrographic surgery (MMS) is the standard treatment for removal of NMSCs.[3,4] When compared to surgical excision and other treatment modalities, MMS offers the best cure rates and is the most cost effective.[5] Consequently, as skin cancer incidence rates continue to dramatically increase, the number of MMS procedures, too, has been increasing. For example, the number of MMS procedures for NMSCs in the Medicare population increased by two times during 2001 to 2006,[6,7] resulting in an increasing financial burden related to health care service and treatments.

MMS is performed in stages, while being guided by the examination for residual tumor in the peripheral (epidermal) and deep subcutaneous (dermal) margins with frozen pathology.

However, preparation of frozen pathology at each stage is time consuming and labor intensive. The preparation usually takes 20 to 60 min per excision,[8,9] during which the patient waits, and the entire cycle is repeated until a tumor-free plane is achieved. Studies have shown that, depending on the setting, more than half of the cases can show residual tumor after the first excision,[10–12] resulting in additional Mohs stages. Consequently, the overall Mohs procedure lasts for at least 1 to 2 h, can take several more hours in some cases, and is tedious and inefficient.

A noninvasive real-time high-resolution optical imaging approach, such as reflectance confocal microscopy (RCM), may help to enhance the Mohs procedure by enabling intraoperative detection of residual NMSC tumor directly in the surgical wound on the patient. RCM has proven to be promising for the detection of BCCs in human skin *in vivo*. Two large clinical studies have reported that BCCs can be diagnosed *in vivo* with a sensitivity of 92% to 100% and specificity of 97 to 88%.[13,14] Furthermore, two small studies have demonstrated the feasibility of detecting residual BCCs on patients following biopsy.[15,16] Another small study reported feasibility for imaging residual BCC tumor in surgically exposed shallow wounds on patients during Mohs surgery,[17] during which aluminum chloride was discovered to brighten nuclear morphology and enhance BCC tumor-to-dermis contrast and detectability.

Aluminum chloride is routinely used for hemostasis on patients undergoing Mohs surgery. Aluminum chloride produces compaction of chromatin,[18–20] which then leads to increased backscatter and brightening of nuclear morphology. This mechanism is similar to that of the well-known brightening of nuclear morphology by "acetowhitening" with acetic acid.[8] In a bench-top concentration-versus-time study on excised tissues, we determined that the optimal contrast is obtained with an aluminum chloride concentration of 35% when topically applied for 1 min.[21] Lower concentrations produce inconsistent brightening

*Address all correspondence to: Eileen S. Flores, E-mail: florese@mskcc.org
†These authors contributed equally.

of nuclear morphology, while higher concentrations tend to dehydrate tissue, produce necrosis, degrade imaging, and affect subsequent pathology.

Compared to imaging *in vivo* for diagnosis, imaging intraoperatively presents some challenges. The skin is not intact and flat but an open (Mohs surgical) wound in the shape of a crater. Tissue bleeds and has to be treated for hemostasis with aluminum chloride and/or electrocautery. Residual tumor must be detected along the peripheral (epidermal) and also the deeper (dermal) margins, including at the base of the wound. Large areas of tissue including the entire surface of the wound must be rapidly imaged and evaluated.

Therefore, following our bench-top study, we tested initial feasibility for imaging under such conditions, in wounds following diagnostic shave biopsies on patients.[21] The wounds formed after shave biopsies are similar to those formed after the staged excisions of Mohs surgery, and hence presented a clinically relevant model for initial testing. Imaging of nuclear morphology and detection of residual BCC tumor in shave biopsy wounds, using aluminum chloride for contrast, were performed; however, the imaging was slow and limited to small areas in shallow wounds. In this paper, we report further progress in the imaging approach (faster, larger areas with video mosaicking, comparison to pathology) and our initial experience with intraoperative testing on patients during Mohs surgery.

2 Materials and Methods

2.1 *Patients*

Patients undergoing diagnostic shave excisions or MMS treatment for NMSC were selected for this study. Prior to enrollment, patients gave consent under a research protocol approved by MSKCC's Institutional Review Board.

2.2 *Instrumentation*

Imaging on patients was performed with a handheld reflectance confocal microscope [Vivascope 3000; Caliber Imaging and Diagnostics (formerly, Lucid Inc.), Rochester NY]. The illumination is with a near-infrared wavelength of 830 nm, and imaging with a gel-immersion objective lens of magnification 30X and numerical aperture of 0.9. The imaging is performed through a lens-to-skin contact cap consisting of a polycarbonate window, which gently flattens and stabilizes the site of interest. The objective lens was designed to use ultrasound gel as the immersion medium between the lens and window, and oil between the window and skin. The optical sectioning is approximately 3 μm and lateral resolution is approximately 1 μm. Compared to that in the earlier microscope (Vivascope 1500) in the initial study,[21] the handheld version has a smaller objective lens with a small and integrated lens-to-skin contact cap. Whereas the earlier microscope required the physical attachment of a relatively large contact ring to the skin, the new handheld version does not. Instead, imaging is performed by gently pressing the contact cap-and-window against the skin, while the microscope is manually translated over the site of interest. This allows for rapid imaging over large areas, including on anatomically difficult-to-access areas of the body.

In each surgical wound, we acquired a combination of image stacks and videos. An image stack is a collection of *en face* optical sections in depth. Each optical section (i.e., image) in the stack displays a 1 mm $\times$ 1 mm field of view (FOV). Image stacks were acquired at the peripheral epidermal and deep dermal margins of each wound. In addition to stacks of still images, we acquired videos along the peripheral epidermal margin at 8 fps rate for durations of up to 1 min at a time.

2.3 *Imaging in Surgical Wounds*

Imaging in the wound was performed on 25 patients immediately after the surgical procedure: 8 patients were shave excision wounds and 17 patients were stage 1 Mohs wounds (Figs. 1 and 2). The wound was immediately swabbed with aluminum chloride (35%) using sterile applicators. Typically, four swabs were applied, each for 15 s, for total time of 1 min. This was previously shown to be the optimum concentration and time to brighten nuclear morphology and enhance contrast of BCC tumors in RCM images.[21] The wound cavity was filled with a sterile gel (Surgilube, Fougera, Melville, NY) and covered with a sterile transparent adhesive dressing (Tegaderm, 3M, St. Paul, MN). A drop of Crodamol STS oil (Croda Inc., Edison, NJ, U.S.A.) was applied over the dressing. Imaging was performed through the dressing. A combination of stacks and videos were obtained in each wound. All images and videos were acquired by a trained clinical imaging researcher (M.C.). Image quality was controlled by gently pressing the integrated lens-and-contact cap and window against the skin (Fig. 1), and acquiring images slowly and carefully while translating on the patient, to minimize blur and artifacts due to patient motion and/or abrupt changes in wound topography.

In intact skin, the device must be held perpendicular to the surface of the skin, gently flattening and providing stability to the entire site of interest, to obtain a good image. However, for surgical wounds, the surface topography of the epidermal and deep dermal margins tends to be somewhat variable. In most cases, Mohs surgeons perform first stage excisions at approximately 45 deg, with the intent to shave a thin layer of tissue. The angle at which the device must be held perpendicular to the margin, in order to obtain full contact, gently flatten, and stabilize

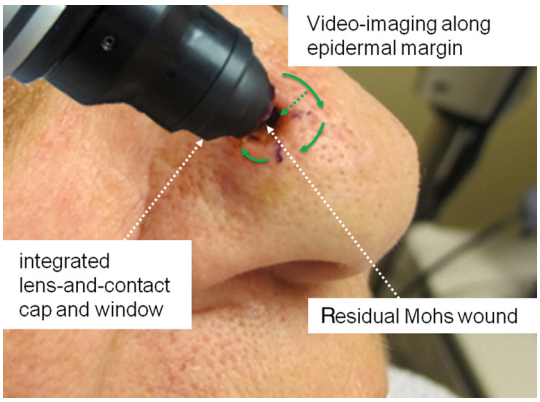

Fig. 1 Reflectance confocal microscopy (RCM) imaging of the residual wound after a Mohs stage 1 excision. Imaging was performed by pressing the integrated lens-and-contact cap and window against the exposed tissue surface in the epidermal and dermal margins. This picture shows video imaging, as performed along the epidermal margin of the wound (green arrows). (More details are in the schematic in Fig. 2.) Wound sizes ranged from 3 to 25 mm in diameter. The entire handheld microscope (not shown) measured 8 $\times$ 24 $\times$ 6 cm.

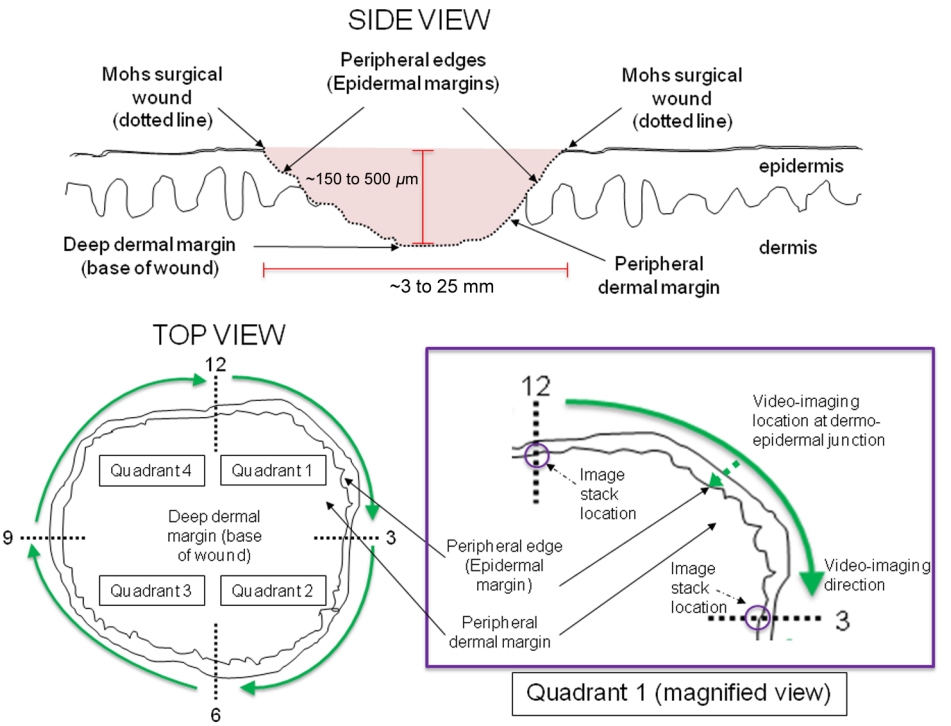

Fig. 2 Crater-shaped topography of a Mohs surgical wound. Imaging was performed in four quadrants: (1) along the peripheral edge, or rim, of the crater (epidermal margin); (2) peripheral dermal margin, below the epidermis; and (3) in the base of wound (deep dermal margin). Image stacks were acquired at the 12, 3, 6, and 9 o'clock positions along the epidermal margin (purple circle), and at the base of the wound. Videos were acquired along the epidermal margin; from the 12 to 3, 3 to 6, 6 to 9, and 9 to 12 o'clock positions (green arrows). The inset (purple box) shows a magnified view of quadrant 1. Note: Figure not drawn to scale.

the site of interest, therefore, varies, depending on angle of excision.

Although imaging was performed in quadrants, to simulate the Mohs surgeon's examination of pathology in quarters, the entirety of each wound quadrant was not imaged. Due to time constraints, the peripheral epidermal and the central portion of the deep dermal margins were mainly selected as the imaging areas (Fig. 2). In particular, the upper periphery of the deep dermal margin (between the epidermal margin and the central portion of the deep dermal margin) was not completely imaged.

2.3.1 *Image Stacks*

In each wound, a total of five RCM stacks were acquired, each stack consisting of 50 images spaced approximately 3 μm apart in depth, at the peripheral edges (epidermal margins) and the base of the wound (deep dermal margin). As illustrated in Fig. 2, (top view), four image stacks were acquired at the 12, 3, 6, and 9 o'clock positions (represented by the dotted lines), each starting on the surface at the peripheral edge (epidermal margin), up to a maximum depth of 150 μm. Each stack acquired at the epidermal margin comprised images representing the epidermal layer, basal layer, dermal–epidermal junction, and papillary dermis. One RCM stack was acquired, starting on the surface at the base of the wound (deep dermal margin), up to a maximum depth of approximately 50 μm. Each stack acquired at the deeper dermal margin comprised images representing the reticular dermis.

In image stacks, the optical sectioning, resolution, and contrast degrades with depth, i.e., images of the superficial layers which are higher in the stack, appear with higher quality relative to those of the deeper layers, which are lower in the stack. However, the loss of quality still remained acceptable and deeper images were useful for clinical utility.

2.3.2 *Videos*

RCM videos were acquired from 20 surgical wounds. In the remaining five wounds, videos could not be obtained due to either time constraints of the patient or wound location. As illustrated in Fig. 2 (top view), in each wound, 1 to 2 videos were acquired in each quadrant, starting at the 12 o'clock position and traversing in a 360 deg clockwise direction along the peripheral edge (epidermal margin) of the wound. Videos were collected as a single sweep, in one plane, along the periphery of each wound quadrant, e.g., 12 to 3, 3 to 6, 6 to 9, and 9 to 12 o'clock. Each video frame consisted of a 1 mm × 1 mm FOV, which included visualization of all three levels (epidermal, peripheral dermal, and portion of the deep dermal margin) of the wound edge. Videos for smaller wounds (i.e., 3 to 5 mm in diameter) included a relatively larger portion of the deep dermal margin, when compared to larger wounds (>5 mm in diameter). Due to constraints of time, the central portion of the deep dermal margin was not imaged. Therefore, the entirety of the deep dermal margin (and thus, the entirety of the quadrant) was not completely imaged.

Our imaging researcher (M. C.) controlled for video quality by gently pressing and applying constant pressure against the skin while translating the microscope for up to 1 min at a time. Images were acquired slowly and carefully to minimize blur artifacts due to patient motion and/or abrupt changes in

wound topography. Video imaging was performed in one plane along the periphery (epidermal margin) of the wound. For this to happen smoothly, imaging (i.e., focal plane) must be maintained on the surface of the epidermal margin. As the microscope is translated over the lesion, video imaging and acquisition along the periphery can be affected by its topography, shape, and size. Maintaining steady pressure on the surface is ideally necessary; however, human operation can occasionally introduce variability and cause sudden (but usually small) movements away or toward the epidermal margin.

2.3.3 *Conversion of videos into video-mosaics*

Each RCM video was processed into a mosaic to display the area that was imaged. In this paper, we use the term "video-mosaics" to distinguish from our earlier work on creating mosaics of still images on excised tissues.[22,23] Video mosaics enable examination of larger areas of skin. After video acquisition, the individual frames were extracted from the video, and patient identification tags in each frame were automatically cropped using an image processing algorithm developed in MATLAB® (Mathworks, Natick, Massachusetts).

The resulting images were then stitched together using freely available video-mosaicking software called Microsoft ICE.[24] Details for the acquisition and processing of videos and application of the software for imaging skin lesions are reported elsewhere.[25] In order for video images to be stitched into a mosaic, subsections of consecutive frames in the video must be registered. This procedure depends on finding distinctive features that represent each frame. For a smooth video, the algorithm first finds these feature points, and then registers the consecutive frames by matching, aligning, and stitching the frames.

When the operator's translation of the microscope was continuously smooth on the skin, the entire sequence of video frames could be processed. However, when "jumps" occurred between frames, usually due to excessively rapid and/or discontinuous translation of the microscope on the skin, the original video was divided into smaller "sub-videos" between these discontinuities, and each was individually processed to create smaller mosaics of smaller corresponding areas. Depending on the complexity of image features and motion artifacts, it takes 10 to 30 min for the video-mosaicking algorithm to convert a RCM video with approximately 500 frames into a video mosaic.[25]

Video mosaics consisted of a sequence of frames (i.e., images) from each video that were stitched together. Each mosaic displays an FOV that is 1 mm wide with the length dependent on the size of the quadrant (wounds ranged from 3 to 25 mm in diameter). These images consisted of frames collected in a lateral single plane on the surface of the epidermal margin and included visualization of all three levels (epidermal, peripheral dermal, and portion of the deep dermal margin) of the wound edge (Fig. 2). Stitching of images is performed by concatenation along nonoverlapping edges with minimal distortion while avoiding blending, such that image quality, in terms of resolution and contrast, in mosaics is preserved relative to that in the individual frames.

2.4 *Histopathology Slide Preparation*

Histopathology was performed on the excisions. For shave excisions, histopathology slides represented vertically oriented sections that are routinely prepared for diagnosis (Fig. 3). For these cases, the RCM images and videos were compared to all the sections to ensure complete assessment of the imaged surface in the wound. For Mohs stage 1 excisions, histopathology slides represented *en face* frozen sections that are routinely prepared to guide Mohs surgery (Fig. 3). For these cases, the *en face* sections correspond to the same surface in the wound that was imaged. Thus, a direct and close (but not necessarily exact) comparison was possible between the videos, video mosaics, and pathology.

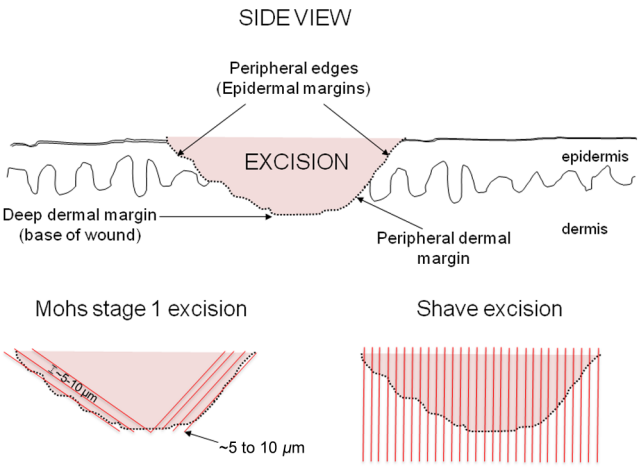

Fig. 3 Histopathology sections (red) used for examination. For Mohs excisions, approximately 5 to 10 μm thin sections spaced approximately 5 to 10 μm apart, are oriented *en face*, parallel to the tissue surface. For shave excisions, the sections are vertically oriented, orthogonal to the tissue surface.

2.5 *Assessment of Reflectance Confocal Microscopy Images/Videos and Histopathological Correlation*

RCM image stacks, videos, and video mosaics were evaluated by two Mohs surgeons (coauthors K. S. N. and A. R.) who are both experienced in reading and analyzing confocal images and mosaics of NMSCs from our previous bench-top studies.[26–30] The overall quality of each RCM image, video, and video mosaic was assessed as clinically acceptable or not. If the quality was acceptable, the image, video, and video mosaic were further evaluated for resolution, contrast, and visualization of nuclear and morphologic detail. The presence of the following structures was assessed: dark nuclear morphology within bright keratinocytes (intact epidermis outside the wound); bright nuclear morphology (exposed peripheral epidermal margin), dermal structures such as collagen bundles, hair follicles, eccrine glands, and inflammatory cells (deep dermal margin) and the presence of residual tumor.

Furthermore, images, videos, and video mosaics were assessed for the presence or absence of tumor in each quadrant, along the peripheral epidermal–dermal junction, peripheral dermal margin, and in the deep dermal margin of each wound against available histopathology slides.

3 Results

We determined that, overall, RCM imaging with aluminum chloride in shave excision and Mohs surgical wounds is feasible (Figs. 4 to 6). Aluminum chloride produced repeatable and

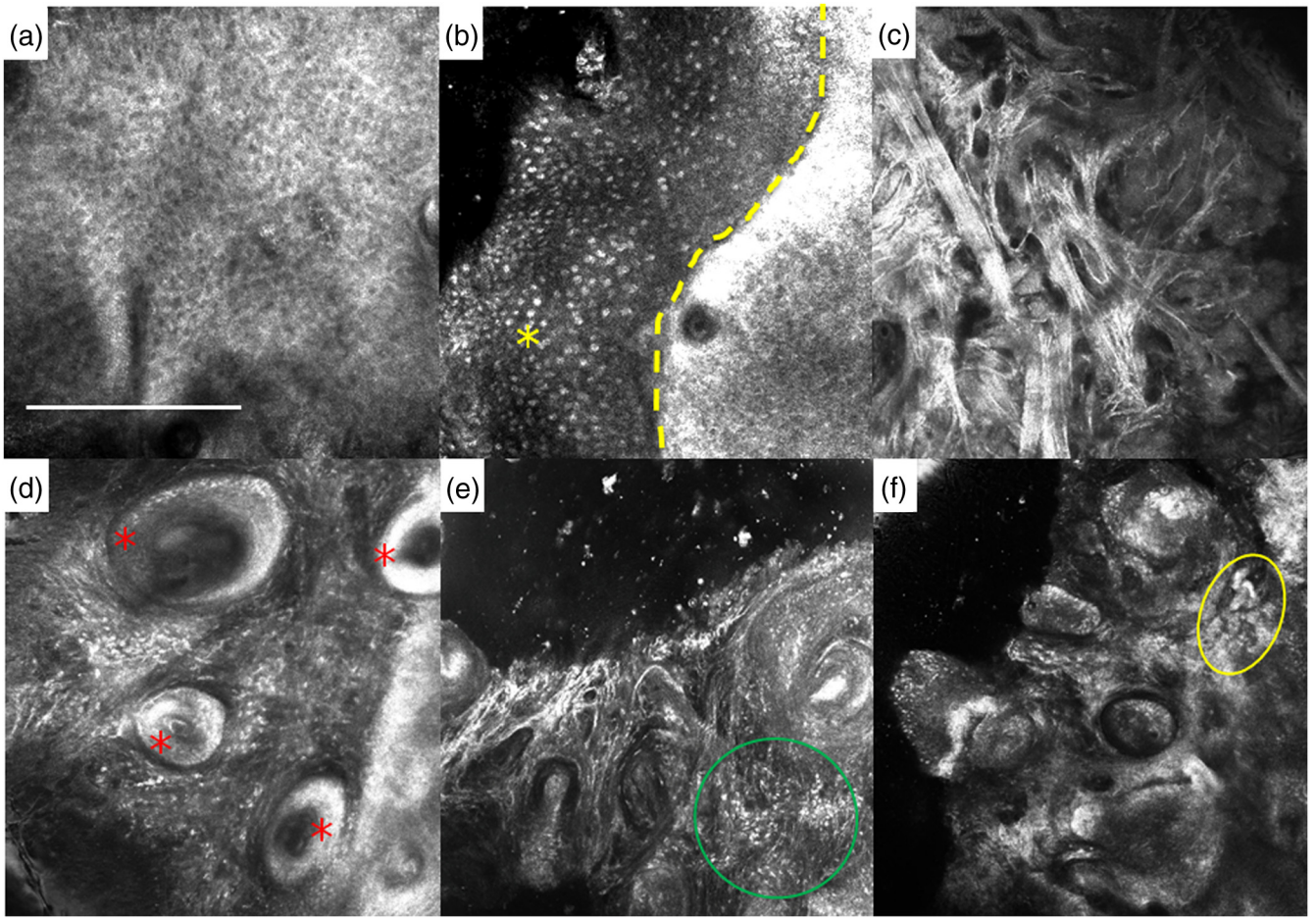

Fig. 4 RCM structures seen surrounding the wound edge (yellow dotted line) and inside the wound: (a) Surrounding intact skin: epidermal keratinocytes seen as polygonal cells with dark nuclei and bright thin cytoplasm displayed in a honeycomb pattern. (b) Exposed epidermis, displaying different pattern: bright nuclei, stained with aluminum chloride, arranged in a cobblestone pattern (yellow asterisk). (c) Deep dermal margin: hyper-reflective fibrillar structures, corresponding to collagen bundles. (d) Hair follicles (red asterisks) and (e) inflammatory cells (green circle), as seen in the deep dermal margin. (f) Sebaceous glands (yellow circle), as seen in the peripheral dermal margin. Scale = 500 μm.

consistent brightening of nuclear morphology and enhanced the contrast and detectability of residual BCC and SCC tumors. In general, we observed the imaging to be of clinically acceptable quality, in terms of resolution and contrast. Nuclear level, cellular level, and dermal morphology, including the presence of adnexal structures such as inflammatory infiltrates, hair follicles, sebaceous, and eccrine glands could be differentiated (Fig. 4). Similarly, the intact skin surrounding wounds and the exposed skin within could be imaged and well differentiated.

Compared to our initial attempt,[21] the acquisition of videos and video mosaicking is relatively more rapid, efficient, and allows for variably shaped and larger regions to be imaged, with the imaging procedure being adaptable to the wound topography. The time required from initial microscope-to-skin contact to the start of image acquisition ranged from 30 s to 1 min. The acquisition of videos required 30 to 60 s for each quadrant, for wounds that ranged from 3 to 25 mm in diameter. For the collected videos, the rate of acquisition ranges from 5 to 24 mm^2 per minute. Fourteen out of the 20 collected videos were converted into mosaics in 10 to 30 min. The remaining six videos did not provide the adequate criteria such as sufficient overlap between their consecutive frames for preparing mosaics, as defined in Kose et al.[25] Nonetheless, these videos were used in the assessments.

3.1 *Evaluation of Surgical Wounds*

Seventeen (68%) out of 25 surgical wounds could be observed with acceptable imaging quality, resolution, and contrast. Relevant structures for the epidermal, peripheral, and deep dermal margins were visible in all of these lesions (Fig. 4). Thirteen (65%) out of 20 videos could be observed with acceptable imaging quality, resolution, and contrast for visualization of nuclear and cellular detail. In five wounds, videos were not obtained due to patient time constraints and wound location.

In the surgical wounds, in which images and videos were found to be of acceptable quality, we identified three margin levels that are relevant for guiding Mohs surgery:

1. *Epidermal margin: at the peripheral edge (rim) of the crater-shaped surgical wound.*

   At the periphery of the wound, bright nuclei, within small polygonal epidermal keratinocyte cells, were seen

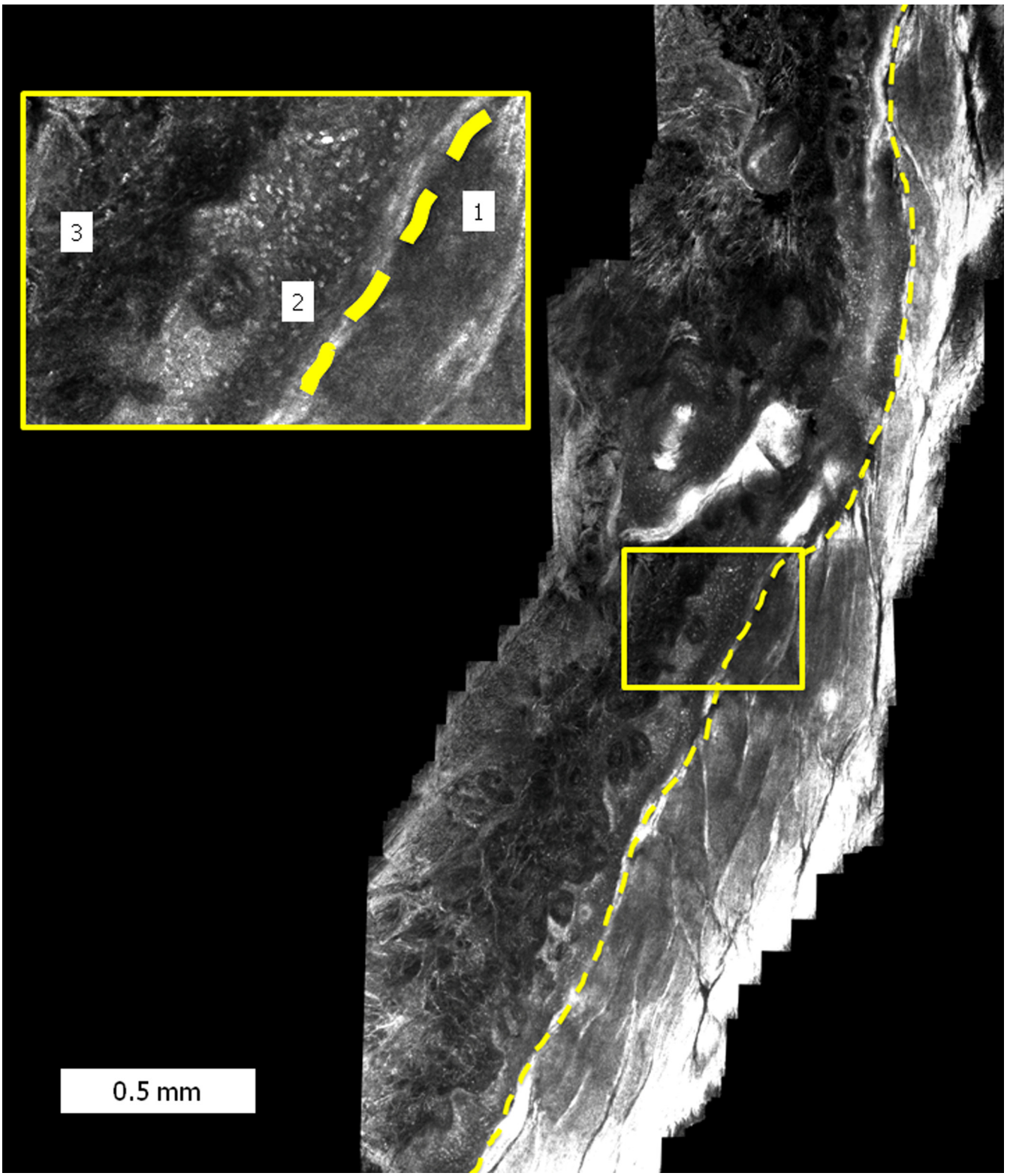

Fig. 5 Video mosaic of a quadrant of a Mohs surgical wound showing: (1) intact skin; (2) epidermal margin; (3) peripheral dermal margin and portion of the deep dermal margin; and the wound edge (yellow dotted line). The inset (yellow box) shows a magnified view of the margin.

in a cobblestone pattern. Each cell was separated by a bright cytoplasmic border. The direct exposure to aluminum chloride, and thus nuclear brightening, was due to the lack of a stratum corneum in the wound. In contrast, the epidermal keratinocytes in the surrounding intact skin were seen as polygonal cells with dark nuclei and bright thin cytoplasm displayed in a honeycomb pattern. The difference between the cobblestone and honeycomb

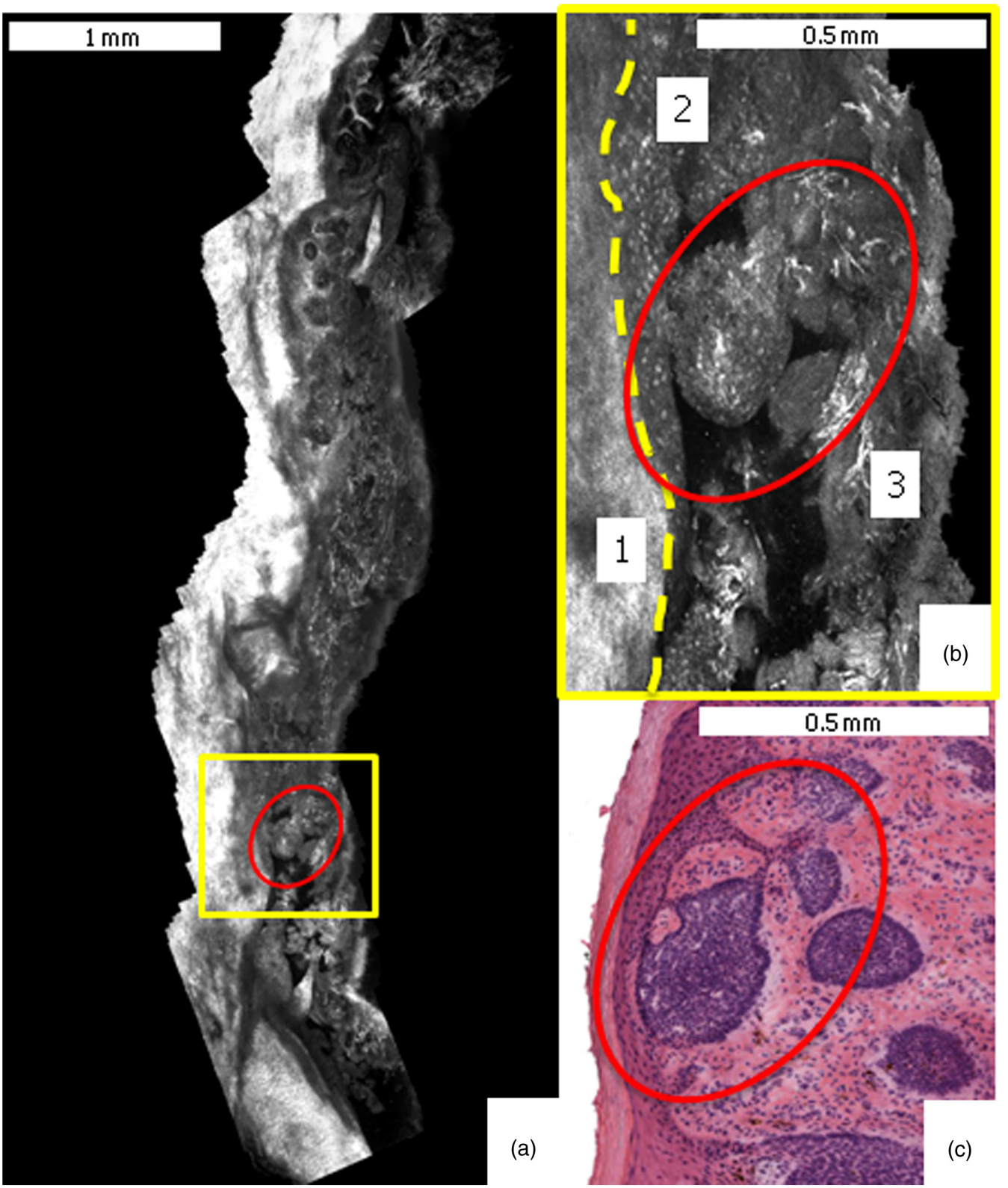

Fig. 6 RCM and histopathology correlation of residual basal cell carcinoma (BCC) in a Mohs surgical wound. (a) RCM video mosaic of a residual wound quadrant. (b) The inset shows magnified view of 1 mm × 1 mm area showing: (1) intact skin; (2) epidermal margin; (3) peripheral dermal margin and a portion of the deep dermal margin; and the wound edge (yellow dotted line). (c) Corresponding en face frozen section, showing nodular BCC (H&E, 20X). Tumor island circled in red.

patterns was easily distinguished and defined the peripheral edges of each wound.

2. *Peripheral dermal margin: at the superficial papillary dermis (below the rim) of the surgical wound.*

   Deeper level images showed the dermo–epidermal junction (DEJ) and dermal papillae were surrounded by a rim of bright cells, contrasting with the dark background. Hyper-reflective web-like structures corresponding to collagen bundles within dermal papillae were seen at deeper levels of the wound.

3. *Deep dermal margin: reticular dermis at the base of the surgical wound.*

   Deeper, still, the shaved wound cavity appeared dark, containing hyper-reflective fibrillar structures, which corresponded to collagen bundles.

   Reasons for unacceptable image and/or video-mosaic quality included artifacts (such as air bubbles, Tegaderm wrinkling) and saturation of brightness which compromised contrast. Other reasons for unacceptable video quality included variability in operator movement, which compromised speed and uniformity of contact pressure against skin.

3.2 *Reflectance Confocal Microscopy and Histopathological Correlation*

In the 17 histopathologically confirmed NMSCs (i.e., the presence of residual tumor after the shave excision or after the Mohs stage 1 excision), we observed correlation between the RCM images/videos and the corresponding histology for the presence of tumor in 15 lesions (12 BCC, 3 SCC). In the remaining two lesions (1 BCC, 1 SCC), the presence of residual tumor was not detectable in the corresponding RCM images and videos. Features of residual BCC or SCC tumor were undetectable due to image saturation and artifacts (such as air bubbles) which compromised the visualization of keratinocytes, cell aggregates, and tumor islands. In both lesions, the video motion was too rapid and did not provide adequate time to demarcate any of the notable features mentioned above. In the lesion with residual BCC, the video spanned several planes in depth and made it difficult to visualize tumor islands within the area of interest. In the remaining eight lesions that showed normal skin, we observed correlation for the absence of tumor (Fig. 5).

In 12 histopathologically confirmed BCCs, the observed features in RCM images were consistent with the histopathology (Fig. 6). Seven lesions described as superficial BCC showed tumor nests with nuclear atypical and bright tumor islands. Tumor aggregates, nuclear polymorphism, and increased nuclear density were seen in the six lesions described as nodular BCC. In one lesion, palisading and clefting were seen. RCM videos showed increased blood flow for two lesions.

In the three histopathologically confirmed SCCs, the observed features in RCM images were consistent with the histopathology. At the level of the stratum corneum, the presence of bright reflective amorphous islands analogous to dry or scaly crust was consistent with the superficial disruption and pleomorphic parakeratosis present in histopathology. RCM features showing atypical honeycombed pattern and disarrangement revealed atypical distribution of keratinocytes and nuclear pleomorphism typically seen at the stratum granulosum layer. At the dermal level, the presence of collagen fiber bundles correlated with solar elastosis and inflammatory cell infiltration. In addition, RCM videos showed increased vascularity with the presence of tightly rounded or S-shaped blood vessels traversing the dermal papillae, perpendicular to the skin surface.

4 Discussion

This paper reports another step in our ongoing development of RCM imaging for intraoperative detection of residual NMSC tumor on patients during Mohs surgery. This study represents our initial experience with imaging in superficial surgical wounds using a newer and smaller handheld microscope, which addresses, to some extent, the major limitations of speed and coverage of area in previous studies.[15–17,21] The results add to our initial findings[21] and show that imaging is possible in the Mohs surgical setting, with aluminum chloride offering repeatable and consistent contrast for nuclear and tumor morphology. Of course, we have shown this in a small study, beyond which this contrast and imaging approach must eventually be tested in a large clinical trial. In fact, we recently initiated the next step, a larger study, involving intraoperative imaging of 60 Mohs surgical wounds. In this larger study, we intend to perform rigorous comparisons to pathology and an initial validation with determination of sensitivity and specificity.

Compared to the large microscope in the initial studies,[15–17,21] the smaller handheld version, with its integrated lens-and-skin contact cap and window, enables easier access into crater-shaped wounds. Images and videos could be taken at the deeper dermal margins, allowing for a relatively more rapid and significant assessment of the wound, with coverage rate of up to 24 mm^2/minute. In addition, video capture allowed the user to rapidly collect images over a larger area of the surgical wound, including the entire epidermal margin. The video acquisition and mosaicking procedure can be adapted to the topography of the wound. (In our earlier studies with the larger microscope, we were limited to mosaicking over predetermined areas of relatively small size and fixed (square) shape. Acquiring the mosaic of a 8 mm × 8 mm region using this technique took approximately 4.5 min, which corresponds to a coverage rate of 14 mm^2/min).

On the other hand, the handheld microscope gives the user flexibility to capture RCM videos over areas of arbitrary shape and size that can be selected in real time during the acquisition. Furthermore, the ability to convert videos into mosaics to display large areas is another useful advance. Maintaining a smooth motion in the lateral direction while translating the microscope on the surface of the wound, and also keeping the focal (imaging) plane constantly on the surface are two of most important requirements for video mosaicking. Any variability in control and pressure against the skin produced "jumps" or discontinuities in the video and blurred images. Whenever this happened, the video was divided into subvideos in which the motion was smooth and the focal depth constant. The subvideos were then individually processed. However, the entire process of finding "jumps" in the video and partitioning it into subvideos is manual and time consuming as of now. Automation of this process will be necessary, such that in the future, the video-mosaicking approach may be implemented within a few minutes. With improvements in speed and area of coverage, this approach may be used to mimic the examination of Mohs pathology, which is usually of 10 × 10 mm^2 of skin with 2X magnification within about a minute. According to our Mohs surgeons (coauthors K.

S. N. and A. R.), for a video mosaic to be high quality, it should satisfy at least three criteria: (1) stitching should be seamless, (2) resolution and contrast of the video mosaic should be comparable to that in the original images from which it was composed of, (3) the details of the cellular and the morphological structures in the original image should be preserved. Based on the analysis given in Kose et al.,[25] in order to obtain a high quality video mosaic, the overlap between the consecutive frames should be at least 25% to 50%. Therefore, it is possible to theoretically achieve a coverage rate of approximately 240 to 360 mm^2/minute, compared to 24 mm^2/minute achieved in this study, with the current imaging configuration (1×1 mm^2 FOV, ~8 frames/second).

Assessment by our Mohs surgeons found that images, videos, and video mosaics exhibited overall clinically acceptable quality with regard to resolution and contrast. Identification of the epidermal, peripheral, and deep dermal margins was feasible due to the immediate recognition of relevant features specific to each region. Furthermore, the presence of artifacts was duly noted, without detracting from any of the image and video assessments of each margin. The images, videos, and video mosaics that were not acceptable were blurred, saturated, and/or contained an abundance of artifact, all of which compromised quality. Saturation in the images and videos appeared to be due to the concentration of the contrast agent, aluminum chloride, which was topically applied prior to imaging. Although 35% was proven optimal for visibility in shave biopsy wounds,[17,21] the tissue conditions in Mohs stage 1 surgical wounds may be more variable. (Such variability is being investigated in the newly initiated larger study.) Nonetheless, despite the compromised quality, recognition of the epidermal, peripheral, and deep dermal margins was still possible. Similarly, the recognition of residual BCC tumor was still feasible despite relatively poor imaging quality in four nodular BCC lesions. This suggests that there may be some leeway for recognition of more amorphous features such as bright tumor islands. However, in two lesions (1 superficial BCC and 1 invasive SCC), when compared to pathology, detailed features such as round inflammatory cells or elongated basal cells, and length of blood vessels were not easily demarcated in the confocal images and videos. In such situations, we may anticipate difficulty in distinguishing challenging cases of BCC or SCC.

In the present study, we utilized the collection of image stacks, videos, and video mosaics to determine the feasibility of intraoperative imaging in Mohs surgical wounds. Because imaging is required only on the surface of the tissue, future imaging protocols may not necessitate the need for still images and stacks, and may be replaced by videos and video mosaics altogether. If the situation warrants it, real-time imaging in the z-depth could easily be done.

Although the small confocal microscope was able to image in previously inaccessible areas, the handheld operation and required manual maneuverability introduced an increase in the learning curve for image and video captures. The microscope, in its present version, still remains too large ($8 \times 24 \times 6$ cm) and somewhat unwieldy to use relative to the size of Mohs surgical wounds (3 to 25 mm in diameter). Also, wrinkling of the sterile Tegaderm, used as a barrier between the surgical wound and objective lens, may manifest as imaging artifacts such as air bubbles or creases. Relevant structures may then be obstructed or misidentified. The use of a disposable tissue cap, instead of Tegaderm, may decrease artifacts without compromising the sterile environment. Similar to our adhesive objective lens-to-tissue contact ring for imaging intact skin *in vivo*, we may need to develop a lens-to-wound contact device, especially to access deeper wounds.

In summary, the limitations at present appear to be more due to the inexperienced and uncontrolled manual operation of the RCM device rather than any fundamental limit on the resolution or contrast of the imaging approach. Furthermore, due to time constraints in the present study, imaging was limited to selected areas of interest, mainly the epidermal margin, peripheral dermal margin, and central portion of the deep dermal margins within the surgical wound. In particular, the upper periphery of the deep dermal margin (between the epidermal margin and the central portion of the deep dermal margin) was not completely imaged. To reduce or eliminate these limitations due to user variability, a much smaller (or, miniaturized) RCM device and a smaller objective lens may offer a solution, especially if coupled with automated and controlled motion for standardized and repeatable translation on the skin. Such a less manual and more automated approach may also ensure complete imaging of the wound, especially the dermal margins, without missing any areas. We anticipate that there will be an optimal size and weight for a smaller RCM device that can be driven with automated control while minimizing motion blur. The design and performance of such a device is the subject of recently initiated development. Beyond the current use of generic (open-source) software, an algorithm to create video mosaics is being specifically designed for this application to significantly reduce processing time. This may also allow for faster imaging and feedback, including, for example, a real-time image/video zoom feature to benefit the Mohs surgeon by providing immediate identification and confirmation of morphologic features within the wound margins.

In conclusion, RCM imaging shows potential as an aid to the surgical management of skin cancer. The reported experience of intraoperative imaging in superficial surgical wounds serves as another step toward the goal of evaluation of residual NMSC margins on patients during surgery. In the long term, our approach may be combined with preoperative detection of lateral margins, to provide a perioperative tool for guiding Mohs surgery. Microscopic approaches that are being investigated for preoperative imaging include RCM, optical coherence tomography, and ultrasound[31–36] Furthermore, microscopic imaging may be combined with macroscopic approaches[37–40] to enable detection over larger areas and/or increased speed. Finally, all of this work in skin and the Mohs surgery setting may serve as an excellent model for optical imaging of residual cancers in other tissues and for translation to other surgical settings.

Acknowledgments

We thank the NIH for funding support (Grant No. R01EB012466 from NIBIB's Image-Guided Interventions program and grant R01CA156773 from NCI). Milind Rajadhyaksha is a former employee and owns equity in Caliber Imaging and Diagnostics (formerly Lucid Inc.), the company that manufactures and sells the Vivascope confocal microscope. The Vivascope is the commercial version of an original laboratory prototype that he had developed at Massachusetts General Hospital, Harvard Medical School.

References

1. H. W. Rogers et al., "Incidence estimate of nonmelanoma skin cancer in the United States," *Arch. Dermatol.* **146**(3), 283–287 (2010).

2. A. Lomas, J. Leonardi-Bee, and F. Bath-Hextall, "A systematic review of worldwide incidence of nonmelanoma skin cancer," *Br. J. Dermatol.* **166**(5), 1069–1080 (2012).
3. F. E. Mohs, "Chemosurgery: a microscopically controlled method of cancer excision," *Arch. Surg.* **42**(2), 279–295 (1941).
4. F. E. M. Mohs and G. R. Mikhail, *Mohs Micrographic Surgery*, W.B. Saunders, Philadelphia (1991).
5. E. P. Tierney and C. W. Hanke, "Cost effectiveness of Mohs micrographic surgery: review of the literature," *J. Drugs Dermatol.* **8**(10), 914–922 (2009).
6. M. R. Donaldson and B. M. Coldiron, "No end in sight: the skin cancer epidemic continues," *Semin. Cutan. Med. Surg.* **30**(1), 3–5 (2011).
7. K. V. Viola et al., "Mohs micrographic surgery and surgical excision for nonmelanoma skin cancer treatment in the Medicare population," *Arch. Dermatol.* **148**(4), 473–477 (2012).
8. M. Rajadhyaksha et al., "Confocal examination of nonmelanoma cancers in thick skin excisions to potentially guide Mohs micrographic surgery without frozen histopathology," *J. Invest. Dermatol.* **117**(5), 1137–1143 (2001).
9. P. Gauthier et al., "Mohs surgery: a new approach with a mould and glass discs: review of the literature and comparative study," *J. Otolaryngol.* **35**(5), 292–304 (2006).
10. M. M. Chren et al., "Tumor recurrence 5 years after treatment of cutaneous basal cell carcinoma and squamous cell carcinoma," *J. Invest. Dermatol.* **133**(5), 1188–1196 (2013).
11. K. Grelck et al., "Incidence of residual nonmelanoma skin cancer in excisions after shave biopsy," *Dermatol. Surg.* **39**(3 Pt 1), 374–380 (2013).
12. V. M. Palmer and P. R. Wilson, "Incompletely excised basal cell carcinoma: residual tumor rates at Mohs re-excision," *Dermatol. Surg.* **39**(5), 706–718 (2013).
13. S. Nori et al., "Sensitivity and specificity of reflectance-mode confocal microscopy for in vivo diagnosis of basal cell carcinoma: a multicenter study," *J. Am. Acad. Dermatol.* **51**(6), 923–930 (2004).
14. P. Guitera et al., "In vivo confocal microscopy for diagnosis of melanoma and basal cell carcinoma using a two-step method: analysis of 710 consecutive clinically equivocal cases," *J. Invest. Dermatol.* **132**(10), 2386–2394 (2012).
15. D. E. Marra et al., "Detection of residual basal cell carcinoma by in vivo confocal microscopy," *Dermatol. Surg.* **31**(5), 538–541 (2005).
16. S. A. Webber et al., "Effectiveness and limitations of reflectance confocal microscopy in detecting persistence of basal cell carcinomas: a preliminary study," *Australas J. Dermatol.* **52**(3), 179–185 (2011).
17. Z. Tannous, A. Torres, and S. Gonzalez, "In vivo real-time confocal reflectance microscopy: a noninvasive guide for Mohs micrographic surgery facilitated by aluminum chloride, an excellent contrast enhancer," *Dermatol. Surg.* **29**(8), 839–846 (2003).
18. S. J. Karlik et al., "Interaction of aluminum species with deoxyribonucleic acid," *Biochemistry* **19**(26), 5991–5998 (1980).
19. S. J. Karlik and G. L. Eichhorn, "Polynucleotide cross-linking by aluminum," *J. Inorg. Biochem.* **37**(4), 259–269 (1989).
20. Y. Matsuzawa, T. Kanbe, and K. Yoshikawa, "Compaction and multiple chain assembly of DNA with the cationic polymer poly(aluminum chloride) (PAC)," *Langmuir* **20**(15), 6439–6442 (2004).
21. A. Scope et al., "In vivo reflectance confocal microscopy of shave biopsy wounds: feasibility of intraoperative mapping of cancer margins," *Br. J. Dermatol.* **163**(6), 1218–1228 (2010).
22. D. S. Gareau et al., "Confocal mosaicing microscopy in Mohs skin excisions: feasibility of rapid surgical pathology," *J. Biomed. Opt.* **13**(5), 054001 (2008).
23. S. Abeytunge et al., "Confocal microscopy with strip mosaicing for rapid imaging over large areas of excised tissue," *J. Biomed. Opt.* **18**(6), 061227 (2013).
24. Microsoft Research, Microsoft Image Composite Editor, 2011, http://research.microsoft.com/en-us/um/redmond/groups/ivm/ICE (30 November 2014).
25. K. Kose et al., "Video-mosaicing of reflectance confocal images for examination of extended areas of skin in vivo," *Br. J. Dermatol.* **171**(5), 1239–1241 (2014).
26. V. Q. Chung et al., "Use of ex vivo confocal scanning laser microscopy during Mohs surgery for nonmelanoma skin cancers," *Dermatol. Surg.* **30**(12 Pt 1), 1470–1478 (2004).
27. Y. G. Patel et al., "Confocal reflectance mosaicing of basal cell carcinomas in Mohs surgical skin excisions," *J. Biomed. Opt.* **12**(3), 034027 (2007).
28. D. S. Gareau et al., "Sensitivity and specificity for detecting basal cell carcinomas in Mohs excisions with confocal fluorescence mosaicing microscopy," *J. Biomed. Opt.* **14**(3), 034012 (2009).
29. J. K. Karen et al., "Detection of basal cell carcinomas in Mohs excisions with fluorescence confocal mosaicing microscopy," *Br. J. Dermatol.* **160**(6), 1242–1250 (2009).
30. B. Larson et al., "Detection of skin cancer margins in Mohs excisions with high-speed strip mosaicing confocal microscopy: a feasibility study," *Br. J. Dermatol.* **169**(4), 922–926 (2013).
31. S. A. Alawi et al., "Optical coherence tomography for presurgical margin assessment of non-melanoma skin cancer: a practical approach," *Exp. Dermatol.* **22**(8), 547–551 (2013).
32. F. Bobadilla et al., "Pre-surgical high resolution ultrasound of facial basal cell carcinoma: correlation with histology," *Cancer Imaging* **8**, 163–172 (2008).
33. A. Jambusaria-Pahlajani et al., "Test characteristics of high-resolution ultrasound in the preoperative assessment of margins of basal cell and squamous cell carcinoma in patients undergoing Mohs micrographic surgery," *Dermatol. Surg.* **35**(1), 9–15 (2009).
34. M. Nassiri-Kashani et al., "Pre-operative assessment of basal cell carcinoma dimensions using high frequency ultrasonography and its correlation with histopathology," *Skin Res. Technol.* **19**(1), e132–e138
35. Z. Y. Pan et al., "In vivo reflectance confocal microscopy of basal cell carcinoma: feasibility of preoperative mapping of cancer margins," *Dermatol. Surg.* **38**(12), 1945–1950 (2012).
36. K. X. Wang et al., "Optical coherence tomography-based optimization of Mohs micrographic surgery of basal cell carcinoma: a pilot study," *Dermatol. Surg.* **39**(4), 627–633 (2013).
37. S.-Y. Jeon, K.-H. Kim, and K.-H. Song, "Efficacy of photodynamic diagnosis-guided Mohs micrographic surgery in primary squamous cell carcinoma," *Dermatol. Surg.* **39**(12), 1774–1783 (2013).
38. E. Tierney, J. Petersen, and C. W. Hanke, "Photodynamic diagnosis of tumor margins using methyl aminolevulinate before Mohs micrographic surgery," *J. Am. Acad. Dermatol.* **64**(5), 911–918 (2011).
39. R. Alkalay et al., "Fluorescence imaging for the demarcation of basal cell carcinoma tumor borders," *J. Drugs Dermatol.* **7**(11), 1033–1037 (2008).
40. M. Carducci et al., "Margin detection using digital dermatoscopy improves the performance of traditional surgical excision of basal cell carcinomas of the head and neck," *Dermatol. Surg.* **37**(2), 280–285 (2011).

Eileen Flores received her MPH degree in epidemiology from New York Medical College in 2010. She has 10 years of clinical research experience in industry (Unilever, Avon) and academia, with design, implementation, and evaluation of skin studies. Currently, as research project coordinator at MSKCC's Dermatology Service, she serves as the liaison between physicians and the optical imaging team, translating RCM technology from bench side to clinic in order to improve the surgical management of NMSCs.

Miguel Cordova is a foreign MD. He has been with MSKCC for the past 10 years, working with 2D/3D digital imaging and reflectance confocal microscopy of skin. He is involved in imaging research: using confocal microscopy in vivo and ex vivo for clinical management and guiding biopsies; delineating margins of lentigo maligna in the MOHs and OR settings; guiding laser ablation treatment of NMSC; mapping of intra-oral cancers; and mapping NMSC therapy in radiation oncology.

Kivanc Kose received his MSc and PhD degrees from the Electrical and Electronics Engineering Department at Bilkent University. His graduate studies were on compression of 3D computer graphics models (MSc) and signal/image reconstruction, enhancement, and recognition frameworks based in sparse signal processing (PhD). He is currently working as a postdoctoral research fellow at Dermatology Service in MSKCC and developing image processing and machine learning algorithms for cancer diagnosis in confocal microscopy images of skin.

Anthony Rossi is a board certified dermatologist with fellowship training in Mohs micrographic surgery and advanced cutaneous oncology from MSKCC and Cornell. His main research focus is to apply RCM technology to image NMSCs to better delineate subclinical margins and guide treatment. Presently, he utilizes RCM to enhance NMSC laser ablation ex vivo and would like to extend this work in vivo: utilizing RCM pre/post ablation to better demarcate tumor boundaries and confirm tumor destruction.

Milind Rajadhyaksha develops, commercializes, and translates confocal microscopes to guide noninvasive diagnosis and to guide therapy (surgery, laser ablation) of skin, head-neck, and breast cancers. Two of his microscopes have been commercialized (VivaScopes, Caliber Imaging and Diagnostics) and are now being used in clinics, with exciting early impact on patient care. His work spans the entire spectrum from laboratory research through commercialization through translational/preclinical studies to clinical implementation.

William Phillips and Kishwer Nehal author biographies are not available.